

**3-D Characterization of Deuterium Ice-Layer Imperfections in
Cryogenic Inertial Confinement Fusion Targets**

Bruce Brewington

Fairport High School
Fairport, NY

Advisor: Dr. R. S. Craxton
Senior Scientist

Laboratory for Laser Energetics
University of Rochester
Rochester, NY

3-D Characterization of Deuterium Ice-Layer Imperfections in Cryogenic Inertial Confinement Fusion Targets

Abstract

Inertial confinement fusion (ICF) is a technique that is being pursued as an option for generating power in the future. Cryogenic targets are important to ICF because they hold the fuel that undergoes fusion reactions. In order for a cryogenic target to undergo ICF, it is important for the target to compress uniformly in all directions. A computer program has been written to characterize defects in these targets. Various imperfections can show up in the ice layer, such as cracks and bubbles, which prevent the target from compressing uniformly. Characterizing imperfections leads to improvements in techniques for producing the targets. The program analyzes a large number of shadowgraphic images, typically 50, viewed from different directions. To locate the imperfections, the program traces light rays from their position in the image back through the target. By combining this information from each of the 50 images, the program creates a 3-D model that shows the locations, sizes and shapes of the imperfections. Conventional tomographic techniques can not be used in this case because the light rays do not travel straight through the target due to refraction.

1. Introduction

One of the most promising techniques for achieving fusion for generating power is Inertial Confinement Fusion (ICF). Using this technique, a powerful laser system irradiates a small target.¹⁻³

A target is a pellet that contains the deuterium fuel for the fusion reaction. A typical cryogenic target is a sphere with a thin plastic outer layer (3 μm), a thick deuterium ice layer (80 μm) and a deuterium

gas center (see Fig. 1).³ These measurements can vary since different sized targets are produced.

To form the ice layer, the target is first cooled to approximately 18° K, which is just below the triple point of D_2 .³ This does not create a uniform ice layer because gravity pulls the deuterium to the bottom when it is in a liquid state. Bubbles may also form while the deuterium is in a liquid state. When the liquid deuterium freezes, cracks may form in the ice. The target undergoes this process inside a layering sphere.⁴ This is a sphere with a hole to insert the target and viewing windows. A low-power IR laser beam is injected into the layering sphere through a small optical fiber and bounces off the walls of the layering sphere. The target is uniformly irradiated from these diffuse reflections, and is constantly losing heat to the cold, surrounding gas. The heating from the IR laser beams causes vaporization to occur on the inner-ice layer. The thicker portions of the ice layer experience more vaporization because they absorb more heat. The deuterium is

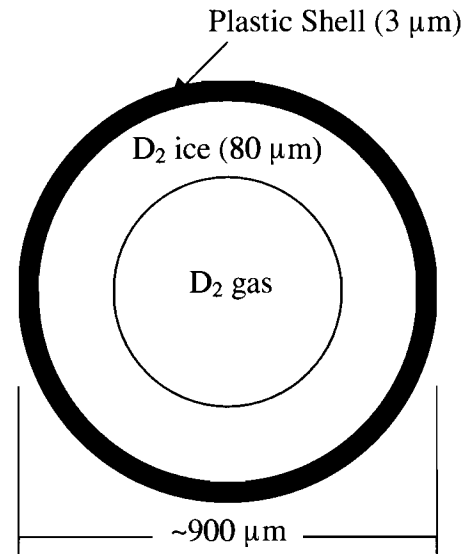


Fig. 1: Slice through a cryogenic target showing its contents.

constantly vaporizing and condensing back on the inner-ice layer. This process continues for about 24 hours and approaches an equilibrium state where the ice layer is uniform.

The high-power laser system delivers energy to the target through many laser beams positioned evenly around the target. The massive amount of energy these lasers deliver causes the outer plastic layer of the target to enter a plasma state and expand outward rapidly. In accordance with Newton's Third Law, an equal but opposite force compresses the deuterium fuel in the target to about 2-3% of its original radius. This creates the high temperature and pressure necessary to make the fusion reactions start. The deuterium ions fuse with each other to form a mixture of helium-3 and tritium ions. These fusion reactions produce energy in the form of high velocity neutrons and protons. Current experiments use just deuterium, but in the future researchers plan to use a mixture of deuterium and tritium because their reaction produces more energy. Deuterium and tritium ions combine to form a helium nucleus (alpha particle) with 3.6 MeV of energy and a neutron with 14 MeV of energy.² Pure deuterium targets are currently used in ICF labs because they are easier to work with than tritium due to tritium's radioactivity.

It is important for the target to undergo a uniform spherical compression to maximize its compression. An imperfection in the target could prevent it from compressing uniformly, ending the fusion reactions prematurely.³ This project involved locating and characterizing major defects such as cracks and bubbles in the ice layer of the target to improve manufacturing techniques.

2. Shadowgraphy

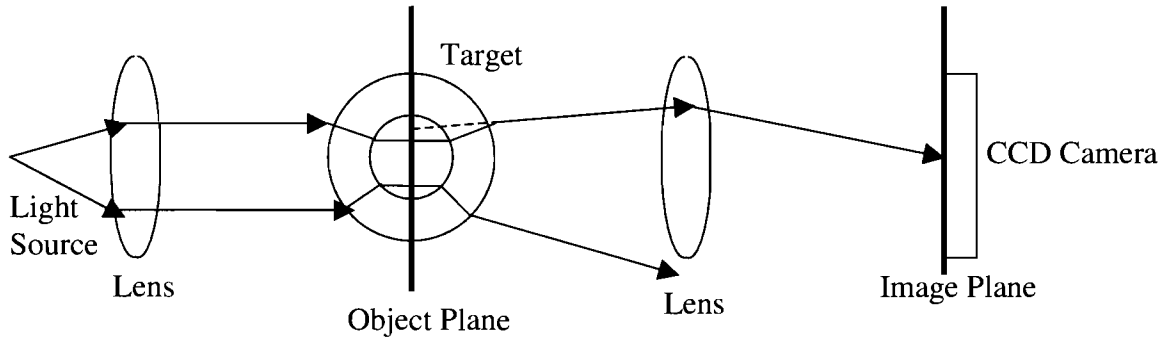


Fig. 2: Schematic of the experimental shadowgraphic imaging system. The dotted line shows where the light ray appears to be coming from. Rays incident too far from the center refract too much to be collected by the lens.

Shadowgraphy is the characterization technique currently used in most ICF labs.^{3,5-9} First, a single collimated light source illuminates a target (see Fig. 2). The light travels through the target and is focused by a lens onto a CCD camera. The lens does not

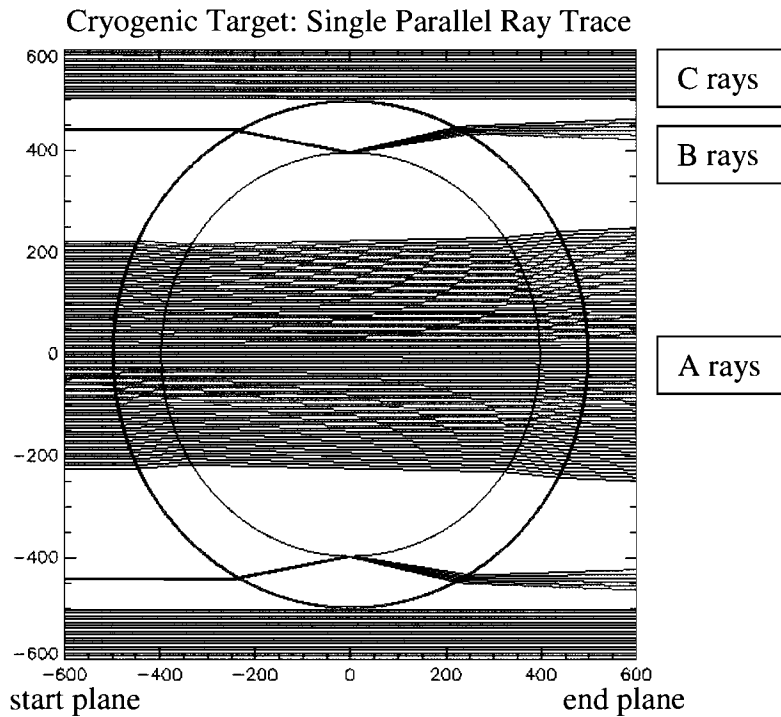


Fig 3: A ray trace demonstrating how shadowgraphy works. Light rays travel from left to right. Only rays collected by the lens are shown. All distances are in microns.

collect all of the light because some rays diverge too far for the lens to be collected.

Rays are labeled based on their path through the target (see Figure 3). The rays

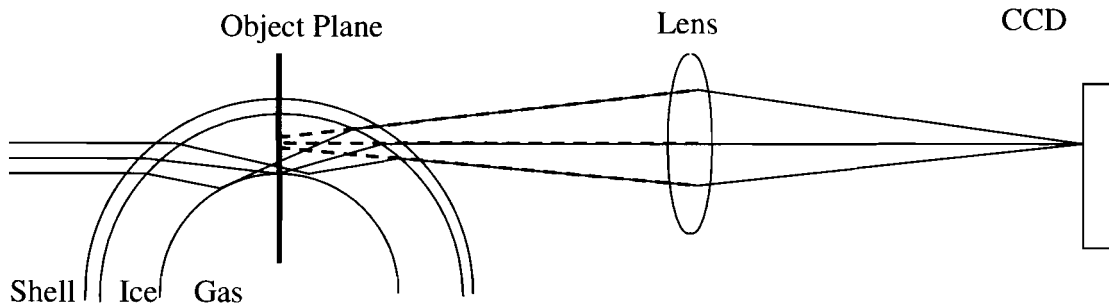


Fig. 4: Diagram showing how the B rays undergo total internal reflection at the ice-gas interface and create the bright ring. From the image on the CCD the B rays appear to come from a tiny spot in the object plane.

that refract through the plastic, ice and gas and are collected by the lens are called A rays.⁸ Some rays refract when they reach the plastic shell and when they reach the ice layer but reflect when they reach the ice-gas interface, and are called B rays (see Figure 4).⁸ When these rays are projected back to the object plane, they appear to come from a very thin ring called the bright ring (see Figure 4). A typical experimental shadowgraphic image containing a bright ring is shown in Figure 5. Computer programs have been written to determine the ice thickness from the bright ring position.⁴ Other programs have been written that trace rays through a target with a non-uniform ice layer and predict what the position of the bright ring should be.^{5,7,9} However, no programs have been reported that analyze defects.

The sample shadowgraphic image in Figure 5 provides a significant amount of information about the target. The colors indicate the intensity of light on the CCD camera with red being bright and blue being dark. The red background is made up of the light rays that did not hit the target. The vertical yellow lines are the spider-silk used to hold

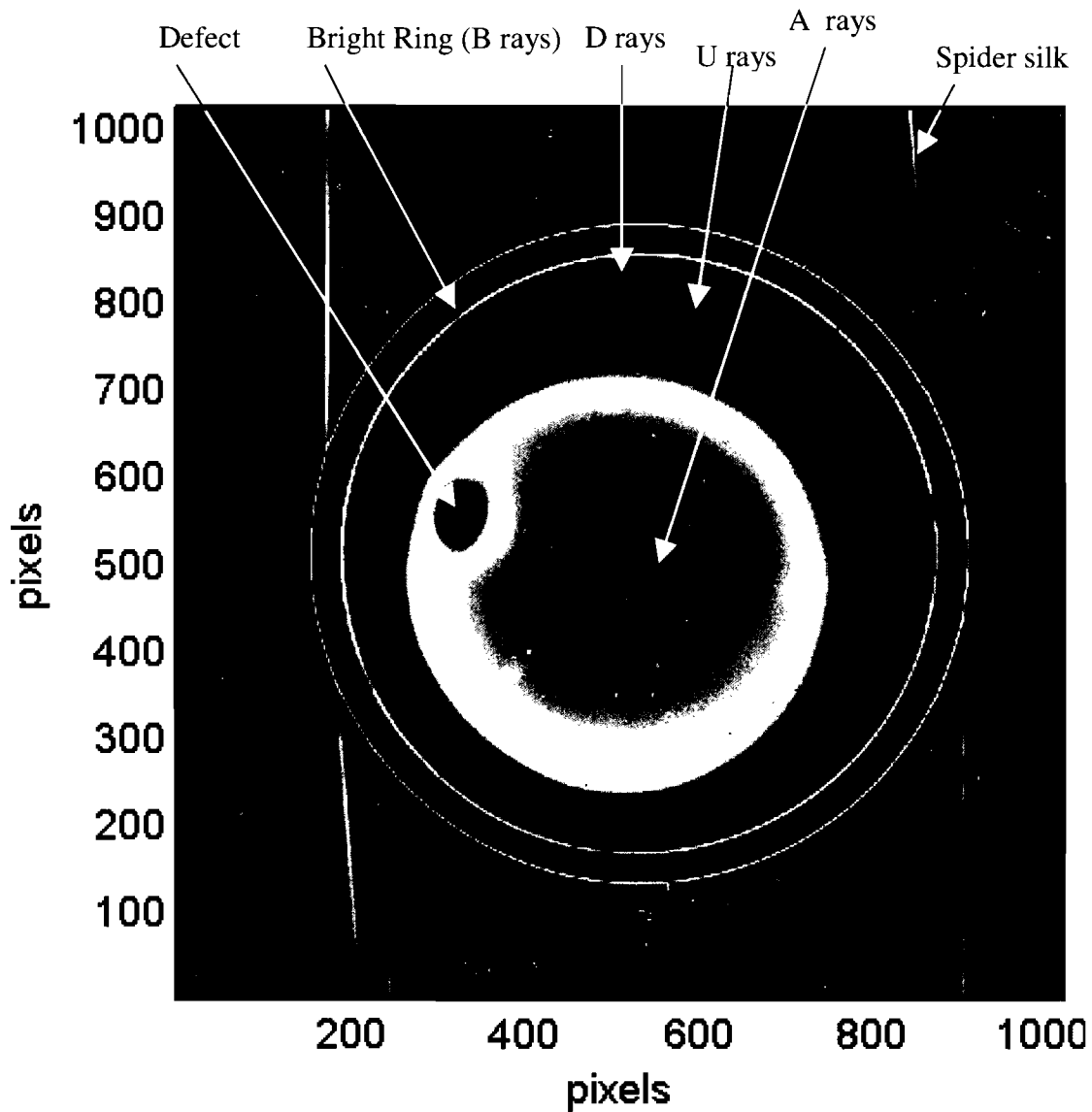


Fig. 5: A sample shadowgraphic image. The colors represent the intensity of the light with red being the most intense and blue being the least.

the target. The large yellow circle and the red area inside it consist of all the A rays. Its size is limited by the size of the lens that collects the light that went through the target. It is off center due to imperfections in the optics that take these pictures, not due to imperfections in the target. The main defect in the image is the large red oval. The brightest of the three rings is the bright ring created by the B rays.

Defects can be seen on shadowgraphic images because the light refracts through

them differently than through the area around them. Sets of 25 shadowgraphic images are taken from each of two cameras located at 12° and 27° above the equator. Each camera takes 25 pictures as the target completes a full rotation about its vertical axis. In each shadowgraphic image the defect is located to the left or to the right of its position in the previous image because the target rotated. When the defect is located near the edge on either the left or the right, the bright ring and the two fainter rings can become broken.

Reconstruction of a 3-D model capable of locating defects from these 2-D images has never been done before. Tomographic techniques can not be used to solve this problem because refraction prevents light from traveling straight through the target. The new program presented here allows the size, shape and location of defects to be estimated accurately.

2. The Program

This project involved developing a program that produces a 3-D model of the target showing the location and approximate size of the imperfections. The 3-D model is based on information from 50 shadowgraphic images taken from different angles. Each shadowgraphic image is displayed on the screen, one at a time. The user flags the areas that have defects on each picture. Based on what the user flags, the program uses an algorithm to find a large number of points that are not part of the defect. The paths of these points are traced back through the target and recorded in a 3-D array representing the target. Combining this information from each of the fifty views creates a 3-D model. This model is viewed in horizontal slices, which can be used to measure the size, shape and location of the defect.

2.1 Input

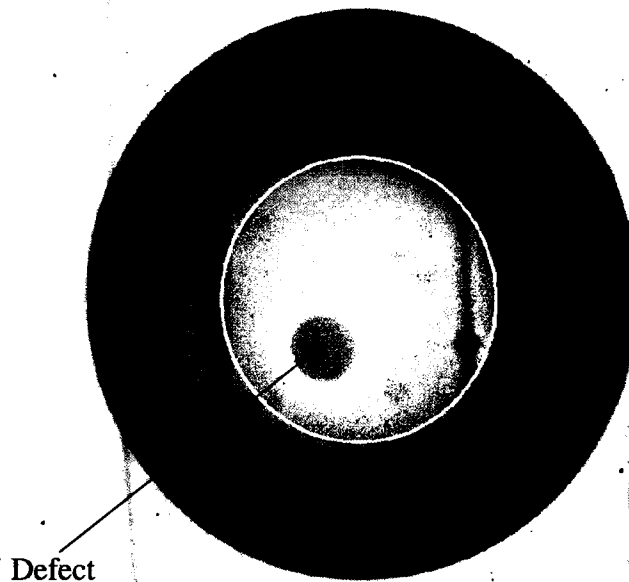


Fig. 6: Screen shot showing how a polygon is drawn around the defect.

The program utilizes data from 50 shadowgraphic images taken from different angles to form the model. Image information including the camera angle, the center of the target in the image and the conversion from pixels to microns is read in from several files. The program reads in and displays the shadowgraphic images from a file. Once the picture is displayed, the user has the option of flagging defects in the paths of the A rays. The user selects the defect on each picture by drawing a polygon around it (see Figure 6). The user's clicks define the vertices of the polygon. There is a feature that allows the user to adjust the positions of the vertices. The default setting disables the adjustment feature to make the interface simpler. The user can draw any number of polygons.

Next, the user has the option of flagging defects shown in the bright ring. These are selected by clicking the beginning and end of the defect on the ring (see Figure 7). The program flags all the points along the ring between these two points. The user is also able to mark any number of defects in the bright ring.

The last piece of information the user supplies is a point from the A rays which does not show a defect. Based on this point, the program uses a recursive function to find a large number of points in the area bounded by the polygons

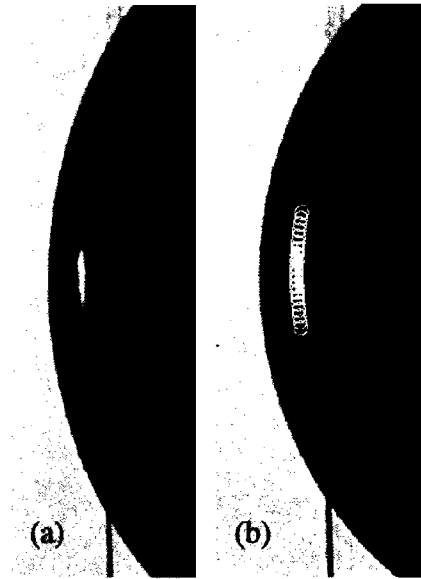


Fig. 7: (a) shows a defect in the bright ring. (b) shows that the area has been flagged.

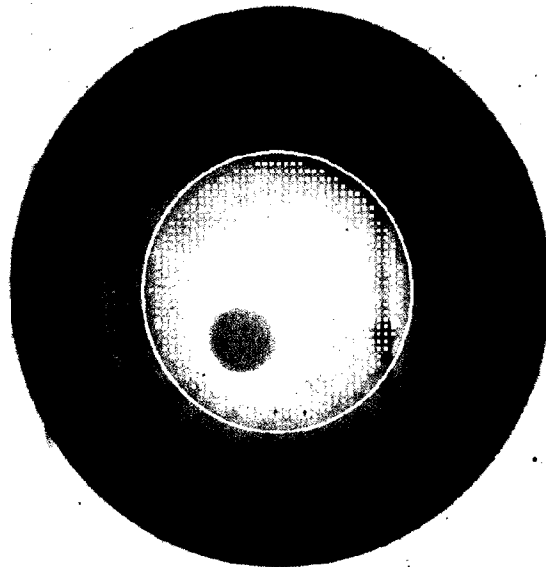


Fig. 8: Screen shot showing a dot at each point that will be traced back.

drawn earlier. This function acts like a fill function. These are the points for which paths will be traced back later (see Figure 8). If there are multiple areas of good points that are not connected to each other, the user can use the fill function multiple times to include all the good points.

2.2 Tracing Rays Back

Another program traces a set of rays with different starting radii forward through the target⁸ and outputs results to a file. A table of each ray's initial radius (R_0 in Figure 9) and its radius in the object plane (R_7 in Figure 9) is created. The ray's radius is the

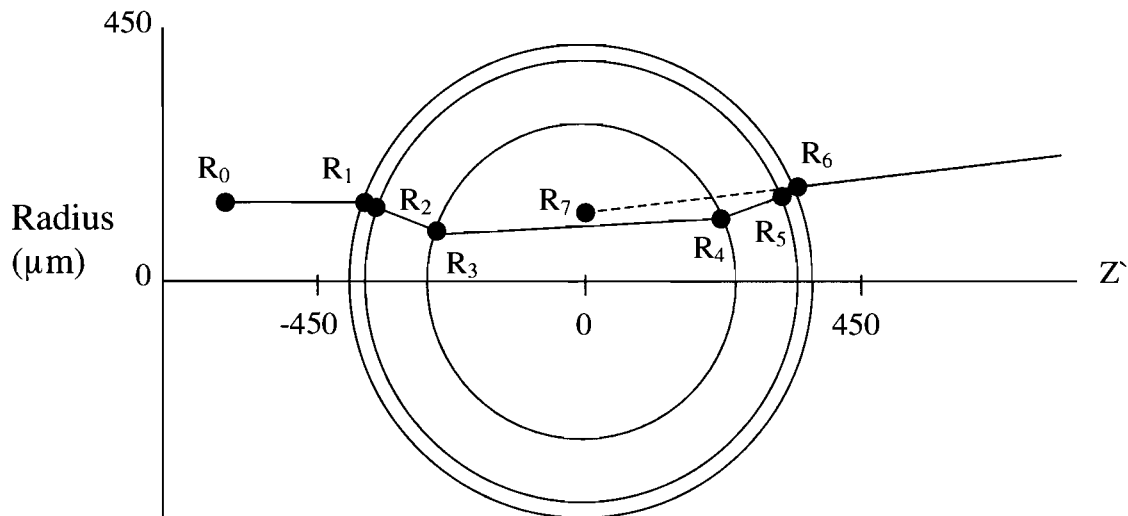


Fig. 9: Diagram showing the path of one ray through the target. R_7 is the radius when the ray is projected back to the object plane ($z=0$). The center line represents a ray that passed straight through the center of the target.

distance from a ray that was initially parallel to it and that traveled straight through the center of the target. Additional tables are created which store the complete path (R_0 - R_6) of each ray based on its initial radius (R_0). Using these tables, the program is able to

analyze the path of any ray. For each point being traced back, the program calculates its radius in the object plane (R_7 in Figure 9) from the image. This is calculated by finding the distance in the image from the center line of the target to the point. Then the program interpolates the initial radius (R_0 in Figure 9) from the first table. From that information, the program can interpolate the path through the target from the second table (all other R 's in Figure 9). Initially, these searches were performed using a linear search. This was later replaced with a binary search to improve the speed.

Using the tables, the ray's path is obtained in the camera frame. The camera frame is a frame of reference where the camera views the target along the z' axis of Figure 9. The problem with this frame of reference is that it is different for each image since the camera moves from picture to picture. To combine the information from the different images, a reference frame is used that is constant for all the images. The ray's path can be converted from the camera frame to the reference frame based on the camera position (refer to Appendix A for a more detailed explanation).

To record the path of each ray the three-dimensional volume containing the target is divided into a $205 \times 205 \times 205$ matrix. Three of these matrices are created to keep track of different information. Each cell of the matrix represents a cube with sides of about 6 microns and keeps track of the number of rays passing through it. The program takes small steps along each ray's

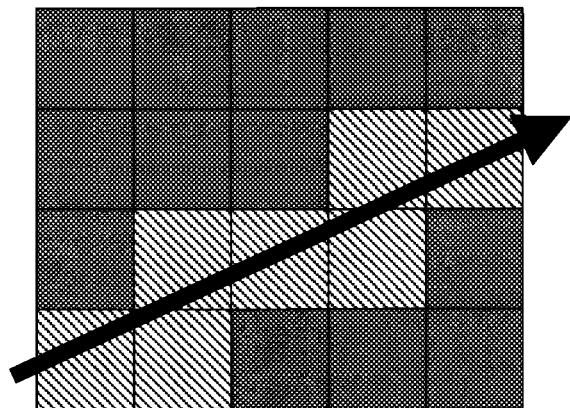


Fig. 10: A two dimensional representation of the way the program tracks the path of each ray. The counter of the red cells will be incremented to show that this ray went through them.

path and at each point it checks whether the ray has moved to a new cell. Whenever the ray moves to a new cell, it increments that cell's counter (see Figure 10).

The first matrix records the paths of the A rays that did not pass through any defects. The second matrix keeps track of the paths of the B rays that did not pass through a defect. The third matrix records the paths of the B rays that did pass through a defect. Each of these matrices is written to a file so that the results are saved. These three pieces of information can be combined to view the data in different ways.

3. Results

The program displays the data from the three matrices through horizontal slices, like a CAT scan. In Figure 11 (a) and (c) the program only displayed the A rays that did not pass through any defects. The dark areas in (a) and (c) indicate that rays were blocked by a defect. This analysis is useful for determining the approximate location of the defect, but it gives no indication of how deep in the ice layer the defect is located. This ambiguity is caused by the fact that a single A ray goes through the target almost head on. This causes it to go through the entire depth of the ice layer. Therefore, if that ray goes through a defect, it is impossible to determine at what depth that defect is located. The B rays, on the other hand, travel through the ice layer obliquely (see Figure 3), giving a strong indication of the depth of a defect. Frames (b) and (d) in Figure 11 show that the defect is on the inner ice surface. Combining the A and B rays that did not pass through a defect provides an estimate of the defect's depth. Although it is difficult to see, there are some lines missing in the B rays in the same area where the dark spot in the A rays occurs. The pattern formed by the B rays has many dark spots in it where no rays passed due to the limited number of camera positions. Each of the lines in (b) and (d)

corresponds to one of the camera views.

A more accurate picture can be found by using the A rays that did not intersect a defect and the B rays that did intersect a defect (see Figure 12). Using this method, the program draws the A rays that do not intersect a defect. Then it draws bright lines where

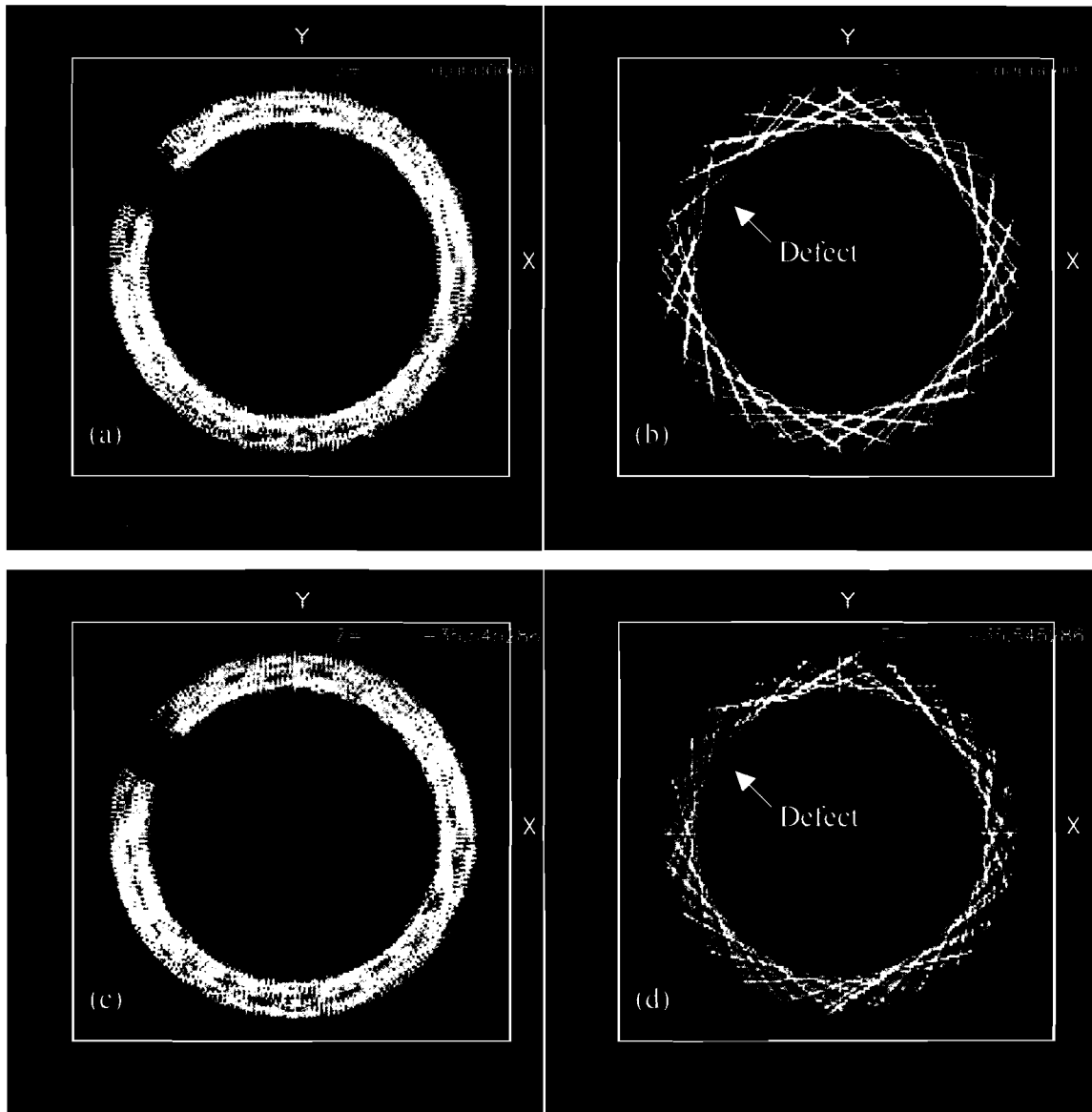


Fig. 11: (a) and (c) show slices through the matrix that recorded the paths of the A rays that didn't go through a defect. (b) and (d) show slices through the matrix that recorded the paths of the B rays that didn't go through a defect. (a) and (b) are horizontal slices at $Z=0$. (c) and (d) are horizontal slices at $Z=-35.5 \mu\text{m}$. Each large white square has sides of $1024 \mu\text{m}$.

there are no A rays that did not intersect a defect and there are B rays that intersect a

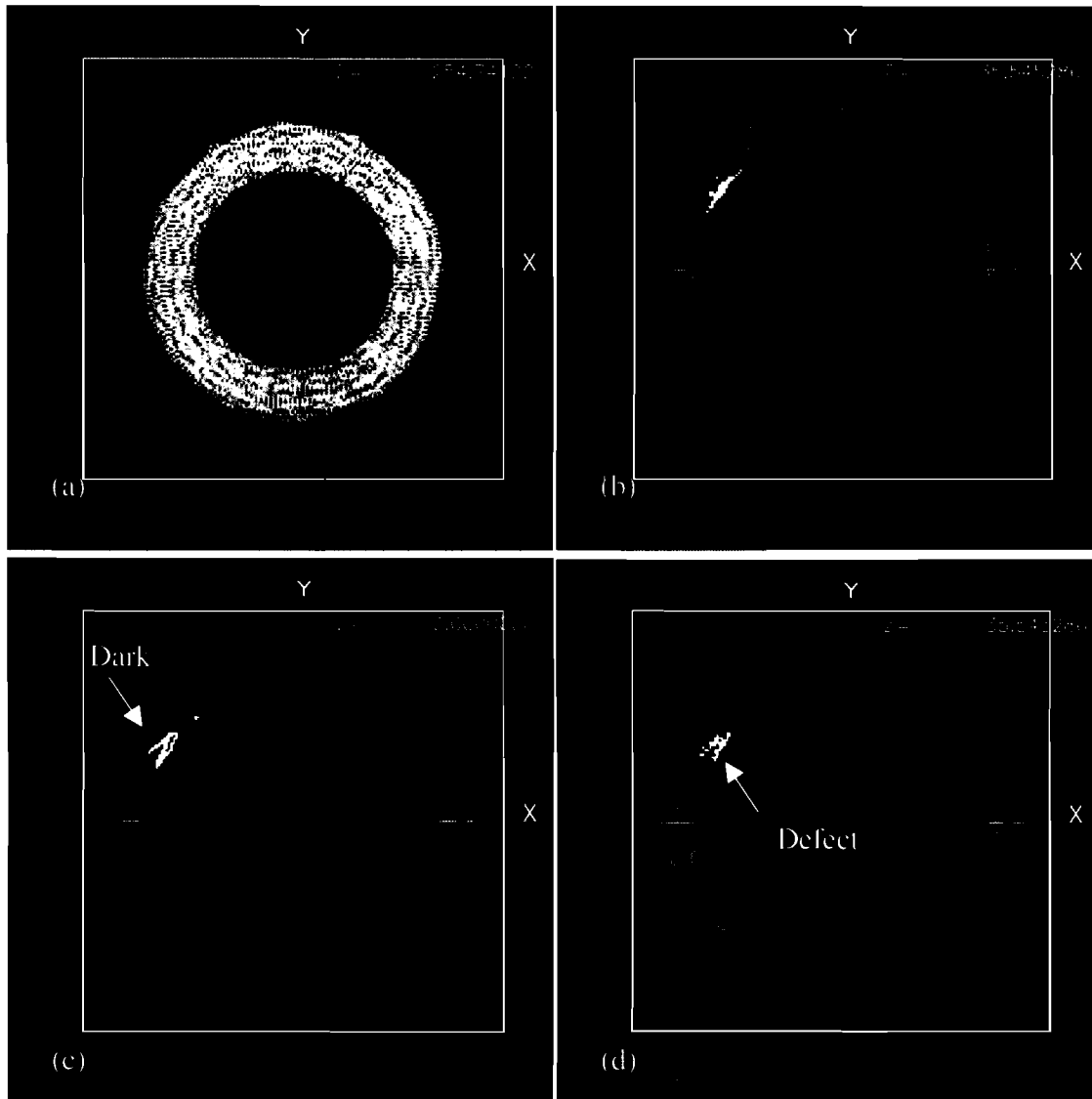


Fig. 12: Four horizontal slices through the 3-D model at Z values of 254.7, 35.5, 0.0 and $-35.5 \mu\text{m}$. (b), (c) and (d) have highlighted areas where there is a defect. There are no defects in (a). The white squares have sides of $1024 \mu\text{m}$.

defect. This technique is much more accurate and easier to read. This method allows the location and size to be calculated from the scale. The resolution of the output is limited by the cell size of the 3-D matrix which is approximately 6 microns at the moment, which is much smaller than the defect. This is enough resolution to estimate the defect's shape.

From the slices through the target shown in Figure 12, it is clear that the defect is on the inner surface of the ice layer. The defect's center is at approximately $(-320, 180, 0)$ μm . It measures about 30 μm into the ice layer, about 70 μm in the Z direction and about 60 μm parallel to the surface of the ice. Defects of this nature have never been characterized in the past.

4. Future Work

In the future, the program will be extended to take into account the fainter rings labeled U and D in Figure 5. Since they take different paths through the target than the B rays, they would improve accuracy in identifying the depth in the ice at which the defect is located as well as the shape of the defect.

Another possible addition would be to increase the resolution of the 3-D model. The resolution could be increased throughout the entire volume or just in the regions where there is a defect. Focusing in on the defect would conserve computer memory. This would provide increased accuracy in the important areas.

The program could also be expanded to trace rays through the defect to compare the intensity perturbations with those seen on the shadowgraphic images. This would give the program the capability to determine whether the defect is a bubble or a dip or some other sort of anomaly. A program exists that determines what perturbations would occur in the bright ring radius because of bumps and dips in the inner-ice surface.⁹ However, nothing has been published that is capable of modeling intensity plots like Figure 5.

5. Conclusion

The program developed in this work is the first program capable of creating a 3-D model of a cryogenic ICF target showing defects in the ice layer. The program was shown to be effective by analyzing a particular target. In this target, the program determined that the defect was on the inner ice surface and was located on the equator. Its dimensions were estimated to be approximately 30 μm deep into the ice layer, 70 μm in the Z direction and 60 μm parallel to the surface of the ice. Imperfections in the ice layer of cryogenic targets are a problem because they cause the target to compress unevenly, which decreases the target performance. Characterizing imperfections in targets will lead to improvements in manufacturing techniques and target quality.

6. Acknowledgements

I would like to thank Dr. Craxton for giving me the opportunity to participate in the High School Summer Research program at the University of Rochester. I would also like to thank him for the hours he spent guiding me through this program as my advisor. Thank you also to Dr. Edgell who provided me with all of my target information. I would also like to thank the other 15 students in the program for becoming such great friends and making this a memorable summer.

7. References

- [1] J. Nuckolls, et al., *Laser Compression of Matter to Super-High Densities: Thermonuclear (CTR) Applications*, **Nature** Vol. 239, pg. 139 (1972).
- [2] R. S. Craxton, R. L. McCrory and J. M. Soures, *Progress in Laser Fusion*, **Scientific American** Vol. 225, pg. 68 (1986).
- [3] C. Stoeckl, et al., *First Results from Cryogenic Target Implosions on OMEGA*, **Physics of Plasmas** Vol. 9, pg. 2195 (2002).
- [4] D. N. Bittner, et al., *Forming Uniform HD Layers in Shells Using Infrared Radiation*, **Fusion Technology** Vol. 35, pg. 244 (1999).
- [5] J. A. Koch, et al., *Quantitative Analysis of Backlit Shadowgraphy as a Diagnostic of Hydrogen Ice Surface Quality in Ice Capsules*, **Fusion Technology** Vol. 38, pg. 123 (2000).
- [6] J. K. Hoffer, et al., *Surface Roughness Measurements of Beta-Layered Solid Deuterium-Tritium in Toroidal Geometries*, **Fusion Technology** Vol. 30, pg. 529 (1996).
- [7] J. A. Koch, et al., *Numerical Raytrace Verification of Optical Diagnostics of Ice Surface Roughness for Inertial Confinement Fusion Experiments*, **Fusion Science and Technology** Vol. 43, pg. 55 (2003).
- [8] S. Jin, *A Ray-Tracing Model for Cryogenic Target Uniformity Characterization*, **2002 Summer High School Research Program for High School Juniors**, Laboratory for Laser Energetics Report 329 (2003).
- [9] J. Sater and D. Bittner, *Shadowgraphy and Spherical Capsules*, **General Atomics Report GA-A23240** pg. 5-5 (1999).

Appendix A- Obtaining the Ray Path in the Reference Frame

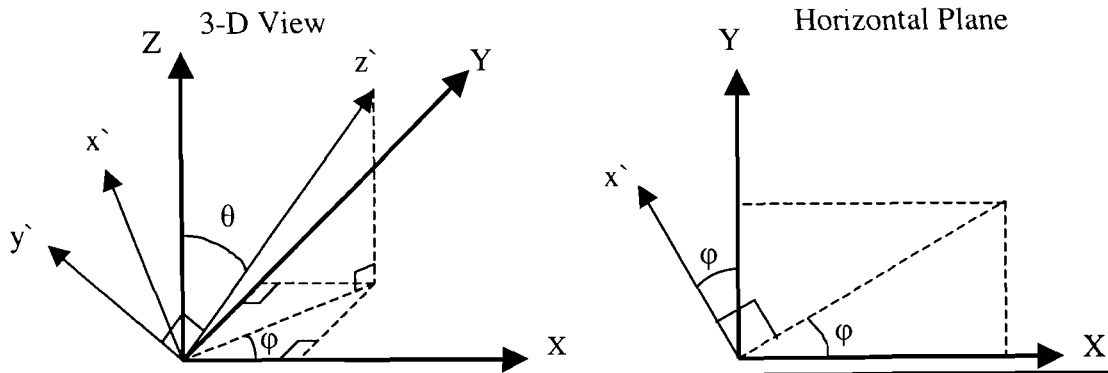


Fig. 13: Diagram relating the reference frame and the camera frame. XYZ is the reference frame and $x'y'z'$ is the camera frame for an image viewed along z' defined by (θ, ϕ) .

The purpose of this appendix is to obtain the path of a ray in the camera frame ($x'y'z'$ in Figure 13) and to convert that path to the reference frame (xyz in Figure 13). Unit vectors \hat{x} , \hat{y} , and \hat{z} correspond to x' , y' , and z' are defined as follows with respect to the reference frame:

$$\hat{z} = (\sin \theta \cos \phi, \sin \theta \sin \phi, \cos \theta) \quad \hat{x} = (-\sin \phi, \cos \phi, 0)$$

$$\hat{y} = \hat{z} \times \hat{x} = (-\cos \theta \cos \phi, -\cos \theta \sin \phi, \sin \theta).$$

Using these conversions, coordinates in x' , y' and z' can be converted to XYZ coordinates. θ and ϕ define the camera location and are read in from an input file.

The coordinates in x' , y' and z' can be determined using the following method. First, the ray's position on the shadowgraphic image is calculated in terms of R_7 and ψ (see Figure 14). Then the ray's entire path (R_0 - R_6 in Figure 9) is interpolated from the table described in Section 2.2 using the method described earlier. These tables provide the z' coordinate as well as the radius at each point along the ray's path. x' and y' can be calculated from this information using the following conversions:

$$x' = R \cos \psi \quad y' = R \sin \psi.$$

This provides sufficient information to convert to the reference frame.

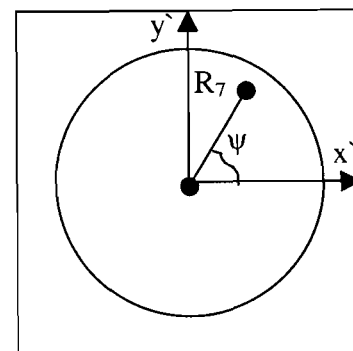


Fig. 14: Diagram showing how R_7 and ψ are obtained from a shadowgraphic image.